Anomalous ambipolar transport in depleted GaAs nanowires

H. Hijazi,[1] D. Paget,[2] A C. H. Rowe,[2] G. Monier,[1] K. Lahlil,[2] E. Gil,[1] A. Trassoudaine,[1] F. Cadiz,[2] Y. André,[1] and C. Robert-Goumet[1]

[1]*Université Clermont Auvergne, Clermont Auvergne INP, CNRS, Institut Pascal, F-63000 Clermont-Ferrand, France*
[2]*Physique de la matière condensée, Ecole Polytechnique, CNRS, Université Paris Saclay, 91128 Palaiseau, France*

(Received 21 December 2021; revised 3 April 2022; accepted 22 April 2022; published 16 May 2022)

We have used a polarized microluminescence technique to investigate photocarrier charge and spin transport in depleted *n*-type GaAs nanowires ($\approx 10^{17}$ cm^{-3} doping level). At 6 K, a long-distance tail appears in the luminescence spatial profile, indicative of charge and spin transport, and only limited by the length of the nanowire (NW). This tail weakly depends on excitation power and temperature. Using a self-consistent calculation based on the drift-diffusion and Poisson equations as well as on photocarrier statistics (Van Roosbroeck model), it is found that this tail is due to photocarrier drift in an internal electric field nearly two orders of magnitude larger than electric fields predicted by the usual ambipolar model. This large electric field appears because of two effects. First, for transport in the spatial fluctuations of the conduction band minimum and valence band maximum, the electron mobility is activated by the internal electric field. This implies, in a counterintuitive way, that the spatial fluctuations favor long-distance transport. Second, the range of carrier transport is further increased because of the finite NW length, an effect which plays a key role in one-dimensional systems.

DOI: 10.1103/PhysRevB.105.195204

I. INTRODUCTION

In the past few years, investigations of transport in semiconductor nanowires (NW's) have gained interest because of potential applications to solar cells [1], lasers [2], and quantum computing [3]. It has been reported recently that GaAs NW's grown on Si substrates have strong potentialities for charge and spin transport [4]. These NW's are *n* doped in the low 10^{17} cm^{-3} range, and are therefore on the metallic side of the Mott transition [5]. They are well adapted for spin transport since the donor concentration nearly corresponds with that of the maximum of the spin relaxation time [6], thus ensuring conservation of spin polarization over large distances.

In such NW's, as shown in Fig. 1, there exist spatial fluctuations of the top of the valence band and of the bottom of the conduction band, induced by statistical spatial fluctuations of the donor concentration [7,8]. Transport of photocarriers occurs through hopping processes, so that it could be anticipated that long-distance transport is difficult. However, it has been shown that carrier transport in this disordered system can occur over distances as large as 25 μm because of the buildup of a large internal electric field [4]. Several phases in the spatial profiles have been observed, due to (i) the dependence of photocarrier mobilities on the electric field [9], (ii) the subsequent spatial redistribution of the Fermi sea for undepleted NW's. However, no interpretation for these results has been proposed.

This work is an experimental and theoretical analysis of charge and spin transport in NW's grown on Si substrates. We have chosen depleted NW so that the charge spatial profiles merely reveal the buildup of the internal electric field since there is no Fermi sea. The spatial charge profile exhibits a relatively fast decrease followed by a slow tail, which weakly depends on excitation power and temperature. As found by numerical resolution of conservation equations, this tail is caused by drift transport in an internal electric field E of a fraction of a V/μm. These results are at variance with the predictions of the usual ambipolar model [10–15] according to which internal electric fields are smaller than this value by two orders of magnitude. Such large internal field is shown to build up for two reasons: first, because of the dependence of the mobility of photoelectrons on the internal electric field [9]; second, the electric field is further amplified by the finite size of the NW. It is anticipated that such large electric fields are specific to one-dimensional systems. For these two reasons, metallic NW's appear as ideal candidates for charge and spin transport.

II. EXPERIMENT

A. Principles

Here we study NW's HVPE-grown on Si(111) substrate using gold catalyst at 715 °C [16]. In order to reduce the surface recombination velocity, the NW's were chemically treated by a low-alkaline (pH $\approx$ 8.5) hydrazine sulfide solution. This produced a negligible NW etching by the solution and covered the surface by a nitride layer so that surface recombination was equivalent to that of the nearly ideal $Ga_{1-x}Al_xAs/GaAs$ interface [17]. After passivation, the NW's, standing on the substrate, were scraped and deposited horizontally on a grid of lattice spacing 15 μm.

The main results presented here were obtained on a depleted NW of length 20 μm and of diameter 100 nm that is smaller than the limit of 180 nm for NW depletion [4]. Also used for comparison was a NW of diameter 500 nm, therefore undepleted, and a depleted NW of diameter identical to the

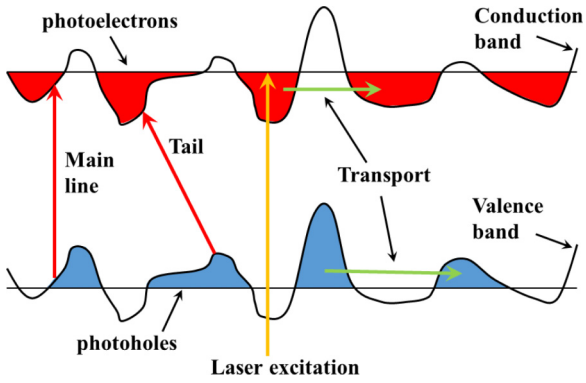

FIG. 1. Spatial fluctuations of the conduction and valence band, caused by statistical fluctuations of the donor concentration. Also shown are the electron and hole transport processes by hopping, and the mechanisms for recombination of the main line and of the tail.

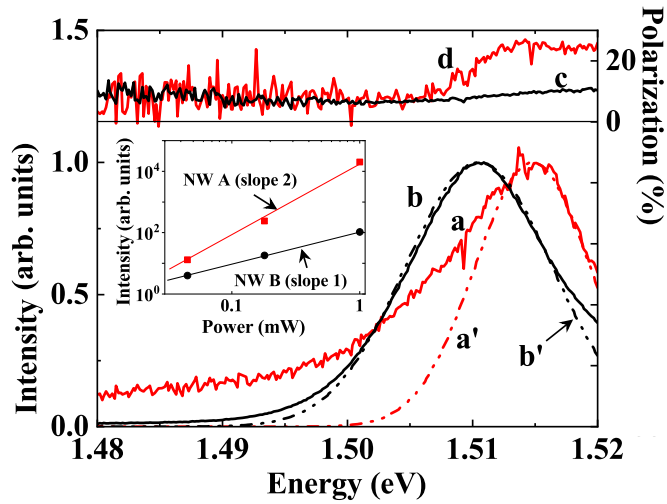

FIG. 2. Curve a shows the NW intensity spectrum at the excitation spot for a small excitation power of 45 μW. Also shown is a Gaussian fit of the main line (curve a′) which reveals a low-energy tail which extends down to 1.48 eV. Curve d shows the corresponding polarization spectrum and reveals a large photoelectron spin polarization of nearly 50%. For comparison, the intensity and polarization spectra of an undepleted NW are shown in curves b and c, respectively. Shown in the inset are the dependencies of the luminescence intensity at the excitation spot as a function of excitation power. As expected from Eq. (1), for the undepleted NW, the intensity is proportional to the excitation power while, for the depleted NW, it is proportional to the square of this power.

main NW, but grown on a GaAs substrate. Such NW is known to be p type, of a doping level equal to several 10^{16} cm^{-3}.

The NW was excited at 6 K by a continuous-wave, laser beam (energy 1.59 eV). The laser was tightly focused to a profile of Gaussian radius $\sigma \approx 0.6$ μm. Since this radius is larger than the NW diameter d, only a fraction of the exciting light impinges on the NW surface. Spatially resolved spectral analysis of the intensity and circular polarization of the luminescence was performed using a setup described elsewhere [4,18]. The observation of transport at large distance from the excitation spot required the monitoring of relatively weak signals. By subtracting parasitic signals, measured by slightly displacing the laser excitation out of the NW, one could monitor physical signals over a dynamic range of three orders of magnitude. Using liquid crystal modulators, the sample was excited with $\sigma^{\pm}$-polarized light and the intensity $\mathscr{I}(\sigma^{\pm})$ of the luminescence components with $\sigma^{\pm}$ helicity was selectively monitored. The luminescence intensity is the sum of these two components and given by

$$\mathscr{I} = K(n + n_0)p, \tag{1}$$

where n is the photoelectron concentration, p is the photohole concentration, and K is the bimolecular recombination coefficient. Here, quite generally, we take a nonzero electron concentration in the dark n_0. The difference signal $\mathscr{I}_D = \mathscr{I}(\sigma^+) - \mathscr{I}(\sigma^-)$ is equal to $Kp\mathscr{P}_i s$, where $\mathscr{P}_i = \mp 0.5$ for $\sigma^{\pm}$-polarized excitation. Here $s = n_+ - n_-$, where $n_{\pm}$ are the concentrations of electrons with spin $\pm\frac{1}{2}$, choosing the excitation light direction as the quantization axis, is the spin density.

B. Results

1. Spectral effects of depletion

For the depleted NW, the intensity and polarization spectra at 6 K and for very small excitation power of 45 μW, corresponding to a power density on the NW surface of 0.15 mW/μm^2, are shown in curves a and d, respectively. The intensity spectrum consists of a main line peaking at 1.515 eV, together with a tail at low energy down to 1.48 eV. As shown in the Supplemental Material [19] and illustrated in Fig. 1, this tail is caused by spatially indirect recombination processes.

For energies larger than 1.51 eV, the polarization has a very large value above 20%, implying a photoelectron spin polarization close to the maximum value of $|\mathscr{P}_i| = 50\%$. This value is relatively large since the Bir-Aronov-Pikus (BAP) process is weak because of the reduced hole concentration [6,20]. Note that the polarization increases near 1.504 eV, which coincides with the onset of the Gaussian component of the intensity spectrum. This is because the electron quasi-Fermi level lies above the minimum of the conduction band fluctuations so that electrons below this level are degenerate.

For comparison, we also show in Fig. 2 the emission characteristics of an undepleted NW. The near-band-gap luminescence and polarization spectra, taken at the excitation spot, are shown in curves b and c of Fig. 2, respectively. As shown in curve b′, the luminescence line shape can be approximated by a Gaussian profile of half-width 6.5 meV. The resulting absence of a spectral tail is at variance with the results of the depleted NW, a fact which is interpreted in the Supplemental Material (see, also, Refs. [4,21,22] therein). Curve c shows the corresponding polarization spectrum and exhibits a maximum polarization of 10%.

A key effect of depletion lies in the dynamic behavior of the luminescence intensity. As shown in the inset of Fig. 2, for the depleted NW, the intensity is proportional to the square of the excitation power. This is expected from Eq. (1) since, for this NW, one has $n_0 \ll n$ so that the excitation power dependence of $\mathscr{I}$ reflects that of the product np. The resulting proportionality of n and p to the excitation power implies that the dominant recombination mechanism is not radiative

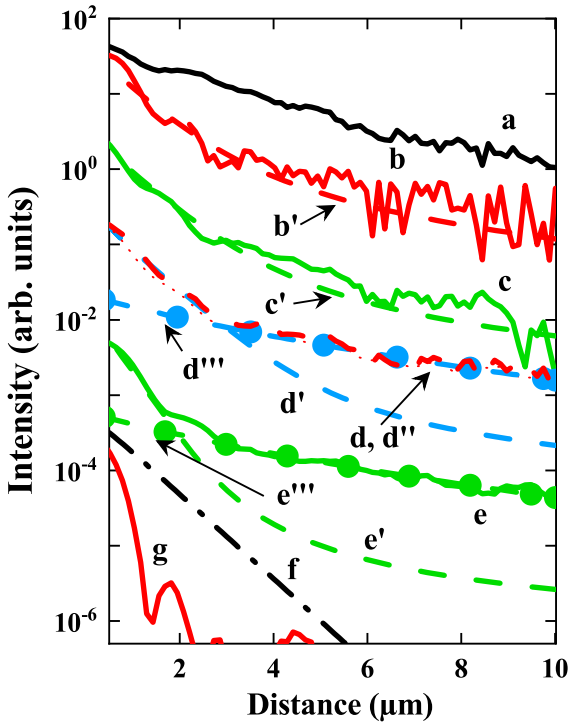

FIG. 3. Curve b shows the intensity spatial profile at 6 K, for an energy of 1.512 eV, for an excitation power of 45 μW. This curve exhibits a slow tail, which is not found for a p-type NW (curve a). These curves extend well beyond the laser profile (shown in curve g), which is an evidence for photocarrier transport along the NW. Shown in curves c and d are the intensity profiles in the conditions of curve b, but for an excitation power of 180 μW and 1 mW, respectively. Curve d$''$ shows the spatial profile of the difference signal, related to the spin orientation, and is almost undistinguishable from curve d. Curve e shows the intensity spatial profile for an increased lattice temperature of 30 K. Curve g shows the profile calculated for an excitation power of 45 μW (same as curve a), but assuming a usual ambipolar transport, i.e., without a dependence of the electron mobility on electric field ($E_e = 0$). Curves b$'$, c$'$, and d$'$ and e$'$ show the corresponding profiles calculated using the model of Sec. III, that is, including a dependence of the mobility on the electric field. While curves b$'$ and c$'$ coincide with the experimental profiles, curves d$'$ and e$'$ underestimate the amplitude of the slow tail. This suggests the relevance of a quasiballistic transport in this large electric field. The corresponding predicted profiles, shown in curves d$'''$ and e$'''$, are obtained using Eq. (13) and coincide very well with the experimental profiles.

electron-hole recombination, but a nonradiative process. In contrast, for the undepleted NW, the intensity increases linearly as a function of excitation power. This is expected from Eq. (1) since, for this NW, one has $n_0 \gg n$ so that the excitation power dependence of $\mathscr{I}$ reflects that of p.

2. *Spatial profiles*

The regime for unipolar transport is first illustrated in curve a Fig. 3, which is the intensity spatial profile for a depleted p-type NW of dimension and passivation similar to those of the main NW. This profile extends well beyond the spatial profile of the laser, shown in curve g. This reveals that carriers excited at the excitation spot have undergone transport over a distance of several μm before recombining. The spatial profile is exponential and close to the predicted profile for one-dimensional unipolar transport (see Supplemental Material of Ref. [4]).

Shown in curve b of Fig. 3 is the intensity spatial profile, taken in the same conditions as curve a of Fig. 2 but for the depleted n-type NW. The spatial profile is very different from curve a, and is therefore characteristic of metallic NW's. It is composed of a rapid decrease up to 2 μm, i.e., over a distance larger than that of the laser profile, with a slower decrease at larger distances. This decrease is superimposed on fluctuations which are reproducible from one curve to the other. The fluctuations in the spatial profile may be caused by inhomogeneities of the surface recombination or by uncomplete spatial averaging of the potential fluctuations shown in Fig. 1.

The observation of the long-distance tail implies that a significant fraction of the carriers escape from the potential fluctuations at the place of excitation and can be transported over large distances. Since hopping processes are easier for electrons than for holes because of their weaker effective mass, there builds up an outwards internal electric field which in turn drives photoholes out of the excitation spot provided its magnitude is comparable to that of the electric field of the fluctuations (of the order of the unscreened effective field near a donor $E_D/a_0^* \approx 0.6$ V/μm, where E_D is the donor binding energy and a_0^* is the effective Bohr radius).

Shown in curves c and d of Fig. 3 are the intensity and difference spatial profiles obtained for a larger excitation power of 180 μW and 1 mW, and corresponding to a power density at the NW surface of 0.6 and 3.5 mW/μm^2, respectively. Comparison between curves b, c, and d reveals that, unlike observed earlier for ambipolar transport in three-dimensional (3D) samples [10–15], the excitation power has little effect on the spatial profiles. Since the increase of excitation power will increase the concentration of carriers trapped in the fluctuations and may lead to screening of these fluctuations, the weak effect of excitation power also suggests that this screening is negligible.

Curve d$''$ shows the profile of the difference signal $\mathscr{I}_D$. This profile is almost undistinguishable from the corresponding intensity profile, curve d. This shows that the photoelectron spin polarization $\mathscr{I}_D/(\mathscr{I}\mathscr{P}_i)$ is constant over the profile. This is expected in our case where the spin relaxation time is large, as suggested by the large photoelectron spin polarization.

Curve e was taken in the same conditions as curve c but at a higher lattice temperature of 30 K, leading to a decrease of luminescence intensity by about one order of magnitude. This curve is quite similar to curve c, implying that temperature has a weak effect on the spatial profile. Such result may appear surprising, in view of the strong temperature dependence of the conductivity reported for metallic systems [5].

III. INTERPRETATION

The results of the preceding section show that depleted NW's on the metallic side of the insulator/metal transition appear as ideal candidates for charge and spin transport.

Transport exhibits a long-distance tail up to 10 μm, mostly limited by the NW end. Because of the weakness of spin relaxation and unlike p-type material, the photoelectron polarization at the excitation spot is close to its maximum value and weakly decreases during transport.

A. Model

In order to interpret these results, calculation of the spatial distributions of electrons and holes was performed using the Van Roosbroeck model [23]. For holes, the drift-diffusion equation is

$$g - K(n+n_0)p - \frac{p}{\tau_{nr}^h} - \vec{\nabla}\cdot[\vec{J}_p/q] = 0. \tag{2}$$

Here g is the rate of creation of electron-hole pairs, q is the absolute value of the electron charge, τ_{nr}^h is the hole nonradiative recombination time, and $\vec{J}_p$ is the hole current. The corresponding spin-unresolved equation for electrons is

$$g - K(n+n_0)p - \frac{n}{\tau_{nr}^e} + \vec{\nabla}\cdot[\vec{J}_n/q] = 0, \tag{3}$$

where τ_{nr}^e is the electron nonradiative recombination time. The quadratic dependence of the spatially integrated luminescence intensity on excitation power, shown in Fig. 2, indicates that nonradiative recombination is dominant over radiative recombination. Since the electron and hole nonradiative recombination terms must be equal after spatial integration which removes the effect of transport, and within the hypothesis of charge neutrality (i.e., that the total photoelectron and photohole charges are equal) one can assume that $\tau_{nr}^e = \tau_{nr}^h = \tau$. The electron and hole currents are given by

$$\vec{J}_n = q\mu_e(n+n_0)\vec{\nabla}E_{Fn} = q\mu_e(n+n_0)\vec{E} + qD_e\vec{\nabla}n \tag{4}$$

and

$$\vec{J}_p = q\mu_h p\vec{\nabla}E_{Fp} = q\mu_h p\vec{E} - qD_h\vec{\nabla}p, \tag{5}$$

where $\mu_{e\,(h)}$ are the electron (hole) mobilities and $D_{e\,(h)}$ are the corresponding diffusion constants. Here E_{Fn} (E_{Fh}) is the energy of the electron (hole) Fermi level with respect to its value at equilibrium. The electronic concentration can be expressed by Boltzmann statistics

$$n = N_c \exp\frac{E_{Fn} - qV - E_c}{k_B T_e}, \tag{6}$$

where k_B is Boltzmann's constant, T_e is the photocarrier temperature, and E_c is the energy of the bottom of the conduction band. As discussed in the Supplemental Material [19], the hole energy distribution for a depleted NW is closer to a Boltzmann one than for an undepleted one. This distribution will be approximated by

$$p = N_v \exp\frac{-E_{Fp} + qV + E_v}{k_B T_e}, \tag{7}$$

where E_v is the energy of the top of the valence band. Here N_c (N_v) is the effective density of states of the conduction (valence) band, and E_c is the energy of the bottom of the conduction band. Here V is the spatially dependent potential, given by Poisson's equation, which can be written, for a spatially homogeneous doping

$$\epsilon_s\frac{d^2V}{dz^2} = q(N_d + p - n - n_0), \tag{8}$$

where ϵ_s is the static permittivity.

For NW's on the metallic side of the insulator/metal transition, transport occurs, as illustrated in Fig. 1, through hopping processes assisted by the electric field. This results in a dependence of the mobility on the electric field [4,9,24], given by

$$\mu_e(E) = \mu_e^* \exp\left[-\left(\frac{E_e}{\sqrt{E^2+E_T^2}}\right)\right] \approx \mu_e^* \exp\left[-\left(\frac{E_e}{|E|}\right)\right], \tag{9}$$

where μ_e^* is the mobility at large electric fields. The electric field E_e is given by

$$E_e = \frac{\Delta_e}{q\delta}, \tag{10}$$

where Δ_e is a characteristic energy, δ is the length of an elementary hopping process, and $E_T = k_B T_e/(q\delta)$. Here, one will use the approximate expression in Eq. (9) since as shown by the weak effect of temperature on the profile, one probably has $E_e \gg E_T$. One may think that the hole mobility also depends on electric field. However, such dependence has no effect on the spatial profiles since hole diffusive and drift currents are negligible with respect to their electronic counterparts and will not be included here [25].

B. Internal electric field within the usual ambipolar model

It is shown here that a simple expression for the electric field can be obtained within simple approximations, within what will be called below the usual ambipolar model [10–12],. Comparison of Eqs. (2) and (3) gives

$$\vec{\nabla}\cdot[\vec{J}_e + \vec{J}_h] = \frac{q(n-p)}{\tau}, \tag{11}$$

where $\vec{J}_e$ and $\vec{J}_h$, given by Eqs. (4) and (5), respectively, depend on electric field via the contribution of drift currents. Within this model one assumes a spatially infinite sample with negligible charge concentrations and electric field at its end. One also assumes charge neutrality ($n = p$). Thus, the sum of electron and hole currents which is zero at infinity, is also zero at all points in the NW, so that

$$\vec{E}[\mu_e(n+n_0) + \mu_h p] = D_h\vec{\nabla}p - D_e\vec{\nabla}n. \tag{12}$$

It will be shown that the usual ambipolar model does not interpret the long-distance tail. However, it allows us to understand the weak dependence of the luminescence intensity profiles on excitation power. Indeed, provided $n \gg n_0$, multiplication of electron and hole concentrations by a common factor will not affect the electric field and therefore the shape of the spatial profile. The weak dependence of the spatial profile on temperature is in agreement with the observed weak temperature dependence of the photoconductivity of disordered systems [9,24]. Such effect can be understood if, in

Eq. (9), $E_T \ll E$. In this case, the electron mobility nonlinearly depends on electric field according to the approximate Eq. (9) which does not depend on temperature. Thus, the sole dependence of the profile lies in the possible temperature dependence of the high-field mobilities μ_e^* and μ_h^*.

C. Anomalous ambipolar transport

Description of the anomalous ambipolar transport requires a self-consistent resolution of the coupled equations (2), (3), (6), (7), and (8). The calculations give the spatial distribution of V, E_{Fp}, and E_{Fn} and subsequently the spatial profiles of n, p, and E. Finally, the spatial profile of the luminescence intensity is given by Eq. (1).

For solving these equations, we applied a Newton-Raphson algorithm, described in Ref. [26], to a NW of length 100 μm with an excitation spot at its middle. For the boundary conditions, one imposed a zero potential at the NW ends and a zero recombination current at the lateral surfaces. In order to avoid divergence, a nonzero value of n_0 and a zero value of E_e were used as a starting point for the calculations. The quantity n_0 was subsequently decreased to 5×10^{13} cm^{-3} and E_e was progressively increased to above 10^{-2} V/μm. The only adjustment in the parameter values was an increase of the high-field mobility values which were $\mu_e^* = 10^4$ cm^2/Vs and $\mu_h^* = 3 \times 10^3$ cm^2/Vs that is slightly larger than mobilities for a degenerate doping level [27]. This is probably because the absence of intrinsic electrons increases the electron and hole collision time. For determining the effective excitation power, we took into account losses by reflection and by uncomplete laser absorption in the NW. The values of the other parameters were found to have a negligible effect on the profile. The electron and hole lifetimes were $\tau = 1$ ns. The electron temperature T_e was taken to 30 K.

In order to show that the slow tail is directly related to the spatial potential fluctuations, we first consider the case of a doping level slightly smaller than the insulator/metal transition, for which the spatial fluctuations of the conduction band minimum and valence band maximum are negligible [28]. Taking $E_e = 0$, the calculated luminescence spatial profile for an excitation power close to that used in curve b is shown in curve f of Fig. 3. The profile exhibits a rapid, approximately exponential, decrease, nearly independent on excitation power and does not interpret the experimental results.

At the excitation spot, the electric field is zero for symmetry reasons. Away from the excitation spot, the electric field is estimated using Eq. (12) to $\approx D_e/(\mu_e L_d)$ where L_d is the exponential slope of the decrease. Using $L_d \approx 0.8$ μm and the Einstein relation $D_e = \mathscr{E}\mu_e/q$, where $\mathscr{E}$ is an energy of the order of the band fluctuation amplitude [9] and assuming charge neutrality, we obtain $E = 3 \times 10^{-3}$ V/μm. This relatively weak value implies that diffusive currents are larger than drift currents and explains the absence of a long-distance tail. It is concluded that NW's of a doping level on the insulating side of the Mott transition do not exhibit the slow tail.

The bottom panel of Fig. 4 shows the calculated photohole concentration profiles for an excitation power of 45 μW and for increasing values of E_e. The top panel shows the corresponding spatial profiles of the electric field. In agreement with the experimental results, and provided $E_e > 10^{-5}$ V/μm,

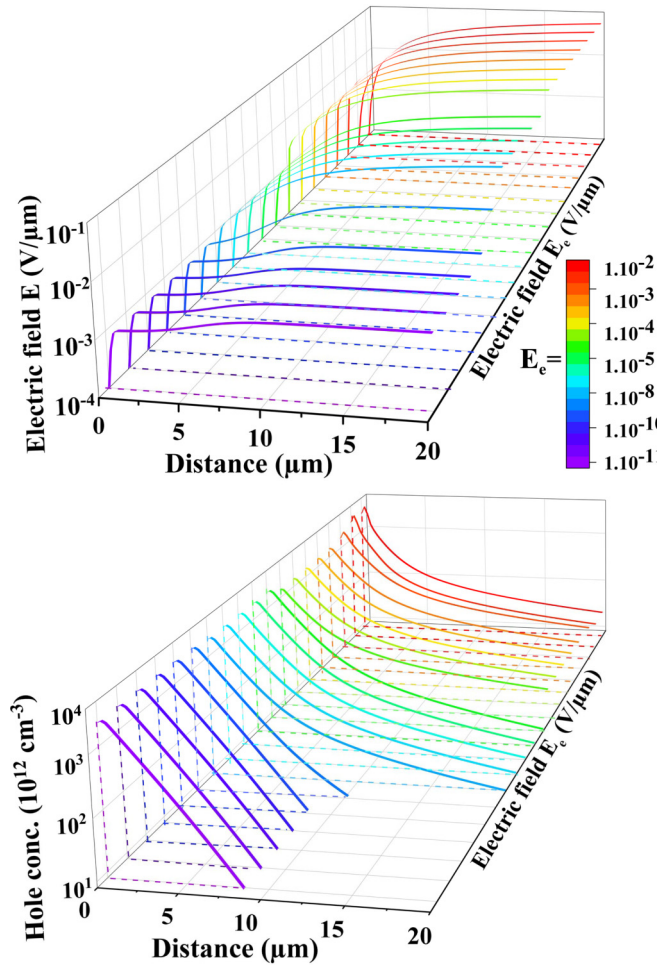

FIG. 4. The bottom panel shows the calculated spatial profiles of the hole concentration for increasing values of E_e. The top panel shows the corresponding spatial profiles of the internal electric field. For a very small value of E_e the decay is rapid, corresponding to the usual ambipolar case as described by Eq. (12). Upon increase of E_e, a tail appears in the charge profile, while a large internal electric field builds up at large distance.

the calculated concentration profiles exhibit a long-distance tail at a distance larger than 5 μm. In this regime, the profile weakly depends on E_e. An estimate of the physical value of E_e can be obtained using Eq. (10) taking $\Delta_e = 1$ m, corresponding to the amplitude of the fluctuations [28] and $\delta_e = 50$ nm. One finds $E_e = 0.2$ V/μm. This is a high estimate of E_e since the electron hopping process may occur over larger distances. However, E_e is in all cases larger than 10^{-5} V/μm so that a long-distance tail should appear.

The internal electric field at a distance from the excitation spot larger than 2 μm is of several 10^{-2} V/μm, i.e., nearly two orders of magnitude larger than for the ambipolar case. This suggests that the tail in the hole concentration profile is caused by outward hole and electron drift in the electric field.

In order to confirm this hypothesis, we have calculated the spatial profiles of the electron and hole currents, using $E_e = 10^{-3}$ V/μm. As seen in Fig. 5, two spatial phases are visible. Up to a distance of 1.5 μm, because of the large concentration gradient, diffusive currents are larger than drift currents. For

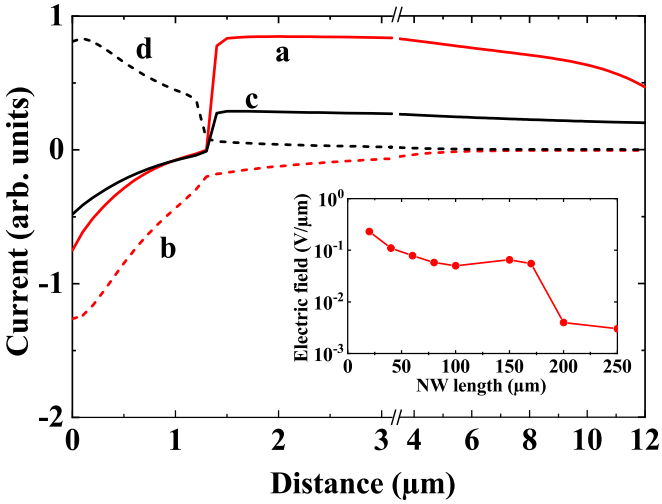

FIG. 5. Spatial profiles of electron diffusive (curve b) and drift (curve a) currents, as well as of the hole diffusive (curve d) and drift (curve c) currents, calculated with $E_e = 10^{-3}$ V/μm. The inset shows the electric field value at 10 μm from the excitation spot, as a function of the NW length. The strong reduction of electric field for a length larger than 150 μm demonstrates the length-dependent transport.

larger distances, drift currents indeed predominate because of the large electric field. These currents explain the presence of charge and spin transport over record distances. Note that the electron drift (curve a) and diffusive (curve b) currents are, as expected, dominant over their hole counterparts (curves c and d, respectively). This justifies the hypothesis taken above of a negligible field dependence of the hole mobility [25].

D. Comparison with the experimental profiles

Curve b′ of Fig. 3 shows the calculated intensity spatial profile, taking for specificity $E_e = 10^{-3}$ V/μm. This curve is in very good agreement with curve b. In the same way, the profile calculated for an increased excitation power of 180 μW very well corresponds with the corresponding experimental profile, shown in curve c.

Curve d′ of Fig. 3 shows the calculated spatial intensity profile for an excitation power of 1 mW. This curve corresponds with the experimental curve d up to 4 μm, while the predicted amplitude of the slow tail is smaller than for the experimental one. We calculate that the electric field at a distance of 10 μm has a very large value of the order of 0.1 V/μm. One may then think that the increase of carrier kinetic energy results in a departure from the hopping transport regime. It has been found earlier that, in such a case, the spatial profile can be interpreted by a model where transport occurs quasiballistically between phonon emission processes [4]. In this case, the unipolar electron concentration is given by $n \approx \exp(-\sqrt{z/\mathscr{L}_e})$, where $\mathscr{L}_e = 2(q/m_e^*)E\tau_{phe}^2$. Here τ_{phe} is the time for phonon emission and m_e^* is the electron effective mass. The hole concentration p is given by the same equation where $\mathscr{L}_e$ is replaced by $\mathscr{L}_h$. Finally, one expects that the luminescence intensity is given by

$$\mathscr{I} \approx \exp(-\sqrt{z/\mathscr{L}_a}), \tag{13}$$

where the ambipolar length $\mathscr{L}_a$ is comparable with both $\mathscr{L}_e$ and $\mathscr{L}_h$.

As shown in curve d‴ of Fig. 3, the intensity for $z > 4$ μm is very well approximated by Eq. (13). One finds that $\mathscr{L}_a$ has the same value of 0.5 μm as for the undepleted NW [4].

Finally, curve e′ shows the intensity profile calculated using $T_e = 60$ m. This curve does not interpret the experimental profile at large distance. Good agreement is reached with the experimental results if (i) the values of the mobilities are large electric field are decreased to $\mu_e^* = 3 \times 10^3$ cm^2/Vs and $\mu_h^* = 5 \times 10^2$ cm^2/Vs, which is an expected effect of the temperature increase, (ii) because of the large internal electric field, one includes ballistic transport. Curve e‴ is calculated using the above model up to a distance of 2 μm from the excitation spot, and using Eq. (13) with $\mathscr{L}_a = 0.5$ μm at large distance.

IV. ORIGIN OF THE LARGE VALUE OF THE INTERNAL ELECTRIC FIELD

It is first shown that the tail in the luminescence spatial profile cannot be explained by the usual ambipolar model [Eq. (12)], even if a field-activated electron mobility is included. In order to evaluate the electric field in this case, one uses $\nabla n/n \approx -(\mu_e E\tau)^{-1}$, as found from Eq. (3) assuming that drift currents are larger than diffusive currents. Further using Einstein's relation, one obtains

$$E^2 \exp[-E_e/|E|] = \mathscr{F}^2 \frac{1 - \frac{\mu_h}{\mu_e}\exp[E_e/|E|]}{1 + \frac{\mu_h}{\mu_e}\exp[E_e/|E|]} \approx \mathscr{F}^2. \tag{14}$$

The electric field $\mathscr{F}$, given by $\mathscr{F}^2 = \mathscr{E}/q\mu_e^*\tau$, is 10^{-3} V/μm, with the parameter values used in Sec. III, and taking $\mathscr{E} = 3$ m. Numerical resolution of this equation shows that the fraction in the right hand is close to unity and can be approximated as shown in Eq. (14). Up to $E_e = 10^{-2}$ V/μm, Eq. (14) has a solution close to $\mathscr{F}$. This value is comparable with usual ambipolar fields. It does not interpret the results and is in contradiction with the starting hypothesis of large drift currents.

This failure is not caused by a possible breaking of the hypothesis of charge neutrality since numerical simulations confirm its validity for calculating the electric field [29], except in a short stretch near the NW end. We propose that the reason why Eq. (14) cannot explain the large electric field is that, because of the slow tail, the photocarrier concentrations and currents near the NW end cannot be neglected. Integration of Eq. (11) between coordinates z and z_0 shows that Eq. (12) must be replaced by

$$\vec{\mathscr{J}}(z) - \vec{\mathscr{J}}(z_0) = D_h\vec{\nabla}p - D_e\vec{\nabla}n, \tag{15}$$

where $\vec{\mathscr{J}}(z) = \vec{E}[\mu_e(n + n_0) + \mu_h p]$ is the sum of drift currents at position z in the slow tail. Here, z_0 is chosen to be sufficiently large so that, as shown in Fig. 5, the diffusive current at z_0 is negligible. Inclusion of the negative term $-\mathscr{J}(z_0)$ in Eq. (15) should result in an increase of the electric field. In order to verify this hypothesis, we have calculated the spatial profiles for increasingly large values of the NW length. The inset of Fig. 5 shows the electric field values at a distance of 10 μm from the excitation spot. Up to a

NW length of 170 μm, the electric field weakly depends on distance and is of $\approx 5 \times 10^{-2}$ V/μm. For a further increase of NW length, one observes a strong decrease of electric field down to 3×10^{-3} V/μm, that is, to a value comparable with the usual ambipolar regime. It is concluded that, at least for the parameter values chosen here, the anomalous ambipolar transport is amplified by NW finite-size effects, provided the NW length is smaller than 170 μm. This length is smaller than the maximum length of usual NW's.

The inset of Fig. 5 shows that the transition between the anomalous and the usual ambipolar transport regimes occurs over a narrow range of 30 μm of width, while the electric field is nearly constant before and after the transition. In the same way, Fig. 4 shows that the transition as a function of E_e occurs over only a factor of 3 of variation of E_e with profiles nearly independent on E_e before and after the transition. As shown in the Supplemental Material [19] for the transition to anomalous ambipolar regime, there also occurs an abrupt transition as a function of excitation power. These features reveal that the transition between the two regimes occurs through a critical process. This can be understood qualitatively, assuming that $E(z) \approx E(z_0)$ and that the photocarrier concentrations at z_0 are fractions of their values at position z [$n(z_0) = \xi n(z)$ and $p(z_0) = \xi p(z)$]. The approximate equation (14) is still valid, provided $\mathscr{F}$ is divided by $\sqrt{1-\xi}$. This induces an increase of $\mathscr{F}$ and therefore of the electric field. This will in turn induce an increase of ξ since this quantity also depends on electric field, according to $\xi \approx \exp[(z - z_0)/(qE\mu_e\tau)]$. The quantity ξ is then closer to unity, which will induce a further increase of electric field.

V. CONCLUSION

It is shown that depleted NW's on the metallic side of the insulator/metal transition (low 10^{17} cm^{-3} range) appear as ideal candidates for charge and spin transport: (i) The spatial profiles of the luminescence intensity exhibit a long-distance tail, weakly dependent on excitation power and temperature, concerning about 10% of the photocarriers and characterized by a decay length larger than 10 μm. (ii) The spin polarization also weakly decreases with distance.

A self-consistent resolution of the drift-diffusion equations, using the Poisson equation and Boltzmann statistics (Van Roosbroeck model) is able to account for these results without extensive parameter optimization. The tail occurs because of photocarrier drifting in an internal electric field as large as 10^{-1} V/μm. At large excitation power and also at increased temperature, the internal electric field becomes very large and carrier transport no longer occurs by hopping but becomes quasiballistic. Two ingredients are crucial for building up a large electric field: (i) the dependence of the photoelectron mobility on internal electric field which strongly increases the electron mobility and results in a field-assisted transport; (ii) critical amplification of these effects caused by the NW finite size.

Note finally that the above reasoning is only valid for one-dimensional systems, i.e., if the lateral dimension is smaller than the typical decay length. Indeed, calculations on 2D systems, with increasing E_e, have not revealed any transition to a slow tail. Since only a limited number of parameter values were chosen, these results need to be confirmed by further experimental and theoretical investigations, which are out of the scope of this work. However, this suggests that the one-dimensional nature of the NW's plays a key role and that NW's are better candidates for charge and spin transport than 2D or 3D systems.

ACKNOWLEDGMENTS

We are grateful to V. L. Berkovits and to P. A. Alekseev for advices in the chemical surface passivation. This work was supported by Région Auvergne Rhône-Alpes (Pack ambition recherche; Convention 17 011236 01-61617, CPERMMASYF and LabExIMobS3 (Grant No. ANR-10-LABX-16-01). It was also funded by the program Investissements d'avenir of the French ANR agency, by the French governement IDEX-SITE initiative 16-IDEX-0001 (CAP20-25), the European Commission (Auvergne FEDER Funds).

[1] P. Krogstrup, H. I. Jorgensen, M. Heiss, O. Demichel, J. V. Holm, M. Aagesen, J. Nygard, and A. F. y Morral, Nat. Photonics **7**, 306 (2013).
[2] X. Duan, Nature (London) **421**, 241 (2003).
[3] J. W. G. van den Berg, S. Nadj-Perge, V. S. Pribiag, S. R. Plissard, E. P. A. M. Bakkers, S. M. Frolov, and L. P. Kouwenhoven, Phys. Rev. Lett. **110**, 066806 (2013).
[4] H. Hijazi, D. Paget, G. Monier, G. Grégoire, J. Leymarie, E. Gil, F. Cadiz, C. Robert-Goumet, and Y. André, Phys. Rev. B **103**, 195314 (2021).
[5] M. Benzaquen, D. Walsh, and K. Mazuruk, Phys. Rev. B **36**, 4748 (1987).
[6] R. I. Dzhioev, K. V. Kavokin, V. L. Korenev, M. V. Lazarev, B. Y. Meltser, M. N. Stepanova, B. P. Zakharchenya, D. Gammon, and D. S. Katzer, Phys. Rev. B **66**, 245204 (2002).
[7] A. L. Efros, Y. S. Halpern, and B. I. Shklovsky, Proceedings of the International Conference on Physics of Semiconductors, Warsaw 1972 (Polish Scientific Publishers, Warsaw, 1972).
[8] B. I. Shklovskii and A. L. Efros, *Electronic Properties of Doped Semiconductors* (Springer, Berlin, 1984).
[9] S. Baranovskii and O. Rubei, *Charge Transport in Disordered Materials*, Springer Handbook of Electronic and Photonic Materials, edited by S. Kasap and P. Capper (Springer, Berlin, 2017), Chap. 9.
[10] R. A. Smith, *Semiconductors* (Cambridge University Press, Cambridge, 1978).
[11] H. Zhao, M. Mower, and G. Vignale, Phys. Rev. B **79**, 115321 (2009).
[12] F. Cadiz, D. Paget, A. C. H. Rowe, E. Peytavit, and S. Arscott, Appl. Phys. Lett **106**, 092108 (2015).
[13] F. Cadiz, D. Paget, A. C. H. Rowe, and S. Arscott, Phys. Rev. B **92**, 121203(R) (2015).

[14] F. Cadiz, D. Lagarde, P. Renucci, D. Paget, T. Amand, H. Carrere, A. C. H. Rowe, and S. Arscott, Appl. Phys. Lett. **110**, 082101 (2017).
[15] D. Paget, F. Cadiz, A. C. H. Rowe, F. Moreau, S. Arscott, and E. Peytavit, J. Appl. Phys. **111**, 123720 (2012).
[16] H. Hijazi, V. G. Dubrovskii, G. Monier, E. Gil, C. Leroux, G. Avit, A. Trassoudaine, C. Bougerol, D. Castellucci, C. Robert-Goumet *et al.*, J. Phys. Chem. C **122**, 19230 (2018).
[17] P. A. Alekseev, M. S. Dunaevskiy, V. P. Ulin, T. V. Lvova, D. O. Filatov, A. V. Nezhdanov, A. I. Mashin, and V. L. Berkovits, Nano Lett. **15**, 63 (2015).
[18] I. Favorskiy, D. Vu, E. Peytavit, S. Arscott, D. Paget, and A. C. H. Rowe, Rev. Sci. Instrum. **81**, 103902 (2010).
[19] See Supplemental Material at http://link.aps.org/supplemental/10.1103/PhysRevB.105.195204 for a brief description about the analysis of the low energy tail in the luminescence intensity spectrum and the abrupt transition to the ambipolar transport regime.
[20] G. L. Bir, A. G. Aronov, and G. E. Pikus, Zh. Eksp. Teor. Fiz. **69**, 1382 (1975) [JETP **42**, 705 (1975)].
[21] A. P. Levanyuk and V. V. Osipov, Usp. Fiz. Nauk. **133**, 427 (1981) [Sov. Phys.–Uspekhi **24**, 187 (1981)].
[22] B. G. Arnaudov, V. A. Vil'kotskii, D. S. Domanevskii, S. K. Evtimova, and V. D. Tkachev, Fiz. Tekh. Poluprovodn. **11**, 1799 (1977) [Sov. Phys. Semicond **11**, 1054 (1977)].
[23] W. van Roosbroeck, Phys. Rev. **91**, 282 (1953).
[24] B. Cleve, B. Hartenstein, S. D. Baranovskii, M. Scheidler, P. Thomas, and H. Baessler, Phys. Rev B **51**, 16705 (1995).
[25] Such result has been verified by introducing a field dependence of the hole mobility, according to $\mu_h(E) = \mu_h^* \exp[-(E_h/|E|)]$ where μ_h^* is the high-field value of the hole mobility, and by performing a numerical calculation of the profile for increasing values of E_h.
[26] P. Farrell, N. Rotundo, D. H. Doan, M. Kantner, J. Fuhrmann, and T. Koprucki, *Numerical Methods for Drift Diffusion Models* (Weierstrasz Institut, Berlin, 2016).
[27] M. L. Lovejoy, M. R. Melloch, and M. S. Lundstrom, Appl. Phys. Lett. **67**, 1101 (1995).
[28] J. R. Lowney, J. Appl. Phys. **60**, 2854 (1986).
[29] Using Poisson's equation and taking $E = 10^{-2}$ V/μm, decreasing with a characteristic distance of 10 V/μm we estimate $p - n \approx 10^{12}$ cm^{-3} that is, 4 orders of magnitude smaller than the carrier concentration at the excitation spot.